Fast at-line characterization of solid organic waste: Comparing analytical performance of different compact near infrared spectroscopic systems with different measurement configurations

Alexandre Mallet, Margaud Pérémé, Lorraine Awhangbo, Cyrille Charnier, Jean-Michel Roger, Jean-Philippe Steyer, Éric Latrille, Ryad Bendoula

To cite this version:

Alexandre Mallet, Margaud Pérémé, Lorraine Awhangbo, Cyrille Charnier, Jean-Michel Roger, et al.. Fast at-line characterization of solid organic waste: Comparing analytical performance of different compact near infrared spectroscopic systems with different measurement configurations. Waste Management, 2021, 126, pp.664-673. 10.1016/j.wasman.2021.03.045 . hal-03204372

HAL Id: hal-03204372
https://hal.inrae.fr/hal-03204372v1

Submitted on 1 Jun 2022

Fast at-line characterization of solid organic waste: comparing analytical performance of different compact near infrared spectroscopic systems with different measurement configurations

Authors: Alexandre Mallet[a,b,c,d,], Margaud Pérémé[a,d], Lorraine Awhangbo[a,d], Cyrille Charnier[c], Jean-Michel Roger[b,d], Jean-Philippe Steyer[a], Éric Latrille[a,d], Ryad Bendoula[b]*

[a)] INRAE, Univ Montpellier, LBE, 102 Av des Etangs, Narbonne F-11100, France

[b)] INRAE, UMR ITAP, Montpellier University, Montpellier, France

[c)] Bioentech, F-11100 Narbonne, France

[d)] ChemHouse Research Group, Montpellier, France

---

[*] **Corresponding author**
E-mail address: alexandre.mallet@bioentech.eu
Full postal address: INRAE-LBE, 102, Avenue des Etangs, F-11100 Narbonne

Abstract

Fast characterization of solid organic waste using near infrared spectroscopy has been successfully developed in the last decade. However, its adoption in biogas plants for monitoring the feeding substrates remains limited due to the lack of applicability and high costs. Recent evolutions in the technology have given rise to both more compact and more modular low-cost near infrared systems which could allow a larger scale deployment. The current study investigates the relevance of these new systems by evaluating four different Fourier transform near-infrared spectroscopic systems with different compactness (laboratory, portable, micro spectrometer) but also different measurement configurations (polarized light, at distance, in contact). Though the conventional laboratory spectrometer showed the best performance on the various biochemical parameters tested (carbohydrates, lipids, nitrogen, chemical oxygen demand, biochemical methane potential), the compact systems provided very close results. Prediction of the biochemical methane potential was possible using a low-cost micro spectrometer with an independent validation set error of only 91 NmL(CH_4).gTS^{-1} compared to 60 NmL(CH_4).gTS^{-1} for a laboratory spectrometer. The differences in performance were shown to result mainly from poorer spectral sampling; and not from instrument characteristics such as spectral resolution. Regarding the measurement configurations, none of the evaluated systems allowed a significant gain in robustness. In particular, the polarized light system provided better results when using its multiscattered signal which brings further evidence of the importance of physical light-scattering properties in the success of models built on solid organic waste.

Keywords

Near infrared spectroscopy; anaerobic digestion; process monitoring; biochemical methane potential; compact systems; measurement modes;

1. Introduction

In anaerobic digestion processes, different organic waste are often co-digested to enhance the production of both biogas and fertilizers (Hagos et al., 2017). A tremendous diversity of waste is concerned by these bioprocesses such as agricultural residues (animal manure, crop stems/stalks, silage), food industry waste (brewery, sugar refinery), urban solid waste, meat waste or catering waste. This implies that these waste cover a large range of biochemical composition and physical properties. Moreover, such properties may fluctuate according to factors such as crop seasonality, transport or storage. This brings important challenges for ensuring the stability of the process and the efficiency of biogas production in digesters (Wu et al., 2019). To answer this, online monitoring of the feeding substrate quality could allow the direct adaptation of the feeding strategy to the feeding substrate quality (Jacobi et al., 2011). However, up to today, this has only been shown to be possible on digesters fed with a single type of substrate (like maize silage), while the usefulness of such system appears greater with important variations of substrate type and quality (Jacobi et al., 2012). In light of this, for co-digestion plants, there is a need for the development of fast and reliable characterization methods that are applicable on highly diverse organic waste.

Near infrared spectroscopy (NIRS), coupled with multivariate analysis techniques (Næs and Martens, 1984), has been successfully used as a fast and robust characterization method of solid organic waste (Skvaril et al., 2017). In the composting process, NIRS was used to monitor the degradation phases of compost (Albrecht et al., 2008), or to predict biochemical characteristics such as the carbon/nitrogen ratio (Vergnoux et al., 2009). In the anaerobic digestion process, the technology was initially used for in-situ monitoring of dry solids (DS), volatile solids (VS), chemical oxygen demand (COD) and volatile fatty acids (VFA) in digesters (Jacobi et al., 2009; Lomborg et al., 2009; Stockl and Lichti, 2018; Wolf et al., 2011). NIRS was then proposed for the determination of biochemical methane potential (BMP) on municipal solid waste (Lesteur et al., 2011), and has since been extended to other types of waste (Doublet et al., 2013; Fitamo et al., 2017; Godin et al., 2015; Triolo et al., 2014; Yang et al., 2021). Today, NIRS appears the most suitable method for predicting BMP on various organic substrates (Rodrigues et al., 2019). More recently, NIRS was used to estimate complementary characteristics such as carbohydrates content, lipid content, nitrogen content, COD, and kinetic parameters (Charnier et al., 2017). In terms of process monitoring, these developments allow time-consuming reference measurements (which last typically one to two months for a characteristic like BMP) to be available in less than five days. Today, what limits the adoption of NIRS in full-scale biogas plants is its low applicability and high costs (Wu et al., 2019). Indeed, freeze-drying and grinding steps are necessary to avoid water and particle size effects in NIRS (Mallet et al., 2021), which currently limits the online applicability of such system. Moreover, the high costs of the spectrometer and the logistics involved in sending the sample at the laboratory still limits a regular and exhaustive analysis of the feeding substrates. Whether NIRS is applied directly on fresh waste or with a prior freeze-drying step, there is a need to develop cheap and reliable instruments which can be used on a wide range of substrate types in order to promote a greater adoption of NIRS in co-digestion plants. This could be addressed by an at-site use of low-cost and compact near infrared (NIR) systems.

In the past few years, the use of NIRS has developed out of laboratories, thanks to important progress in the miniaturization of instruments. In particular, handheld Fourier transform near infrared (FT-NIR) micro spectrometers have appeared in the market, and make use of a micro-electro-mechanical systems-based (MEMS) Michelson interferometer (Beć et al., 2021). While conventional Michelson interferometers are made of discrete elements (including the moving mirror actioned by a motor, the fixed mirror, and beam splitter), MEMS technology enables a monolithic integration of these elements on a single chip, with the particularity that the moving mirror is operated by an electrical signal. Amongst the spectrometers making use of this technology, the NeoSpectra instrument has shown good analytical performance results for soil organic and total carbon content characterization (Sharififar et al., 2019; Tang et al., 2020), or authenticity screening in food (McVey et al., 2021). These compact spectrometers allow the measurements to be performed on site, thanks to their compactness, robustness and cost. However, these compact portable spectrometers tend to have poorer instrument performances than laboratory spectrometer, with lower resolution, spectral range, and signal-to-noise ratio (Beć et al., 2020; Crocombe, 2018). Therefore, the suitability of such systems for the characterization of diverse organic waste still needs to be assessed.

Another aspect of these compact systems concerns their modularity and the possibility of testing different measurement configurations, in order to enhance the measured signal. Indeed, in complex matter such as solid organic waste, the Bouguer-Beer-Lambert law does not hold due to important light scattering (Dahm and Dahm, 2004). To answer this, spectral pre-processing has been proposed to remove both additive and multiplicative effects (Rabatel et al., 2020; Rinnan et al., 2009; Zeaiter et al., 2005) and thus, make the problem linear again. However, other developments have rather focused on enhancing the measured signal directly. A promising optical pre-processing method, based on polarized light spectroscopy (Backman et al., 1999) has been proposed to improve the absorbance signal measurement on such scattering samples (Bendoula et al., 2015; Gobrecht et al., 2015; Xu et al., 2019). Such system has shown analytical performance improvements for soils (Gobrecht et al., 2016), and more recently, for digestate (Awhangbo et al., 2020), but has never been evaluated on solid organic waste. Still in the aim of enhancing the measured spectra, time-resolved spectroscopy shows a promising future : applied to pharmaceutical tablets, collected photons with a particular propagation time were shown to be most informative for quantification (Alayed and Deen, 2017; Johansson et al., 2002). However, the cost of this technology still remains prohibitive for the organic waste management sector. Finally, the measurement mode (at distance or in contact, in reflectance or in interactance) also plays an important role in the final accuracy for estimating biochemical properties (Hemrattrakun et al., 2021; Khodabakhshian et al., 2019; Schaare and Fraser, 2000). Though current used laboratory spectrometers make use of a distance reflectance measurement, a contact immerged probe measurement has been shown to be useful for prediction of parameters on digestates (Awhangbo et al., 2020). Authors observe higher reflectance levels with less noise in the collected spectra, as well as new chemical features which were not apparent in a remote probe configuration. In light of this, it appears that the use of different measurement configurations could enable the calibration of more accurate and more robust NIRS models on diverse solid organic waste.

As mentioned, the applicability of compact and low-cost spectroscopic systems remains to be assessed for biochemical characterization of highly diverse solid organic waste. Moreover, the modularity offered by such compact systems is a unique opportunity to evaluate whether the use of different measurement configurations can help build more robust models. This study aims to assess these two matters by comparing the analytical performances of four different NIRS systems: a standard laboratory spectrometer, a portable spectrometer with two measurement configurations (contact mode and polarized mode), and a micro-spectrometer. For this purpose, measurements were acquired with each system on a selection of solid organic waste. Then, for each spectroscopic system, prediction models for five biochemical characteristics (carbohydrates, lipids, nitrogen, COD and BMP) were calibrated and their performances were compared.

2. Materials and Methods

2.1. Sample preparation and reference analyses

Thirty-three substrates were selected amongst various waste types that have been collected in rural, territorial and industrial anaerobic digestion plants in France. These substrates cover a wide range of biochemical and physical properties: solid cellulosic waste (like silage, cereals and corn cobs), liquid cellulosic suspensions (such as manure), liquid fat suspensions (catering waste or biowaste), sweet emulsions (such as lactoserum), or protein and fat solid pastes (such as egg waste or cacao butter). The visual aspect of some of these substrates in raw form is presented in Appendix A.

For spectral measurements, each substrate sample was freeze-dried and ground to 1 mm. The dataset is fully described in a data paper [On-site substrate characterization in the anaerobic digestion context: a dataset of NIR spectra acquired with four different optical systems on freeze-dried and ground organic waste – this data paper is submitted jointly with this article, reference will need an update after reviewing] and available online [https://doi.org/10.15454/SQQTUU].

Biochemical characterization of substrates was obtained by using a NIRS calibrated model (Charnier et al., 2017), with errors on independent test sets of 53 $mg(O_2).gTS^{-1}$ for carbohydrates content, $3.2*10^{-2}$ $g.gTS^{-1}$ for lipids content, 8.6 $mg.gTS^{-1}$ for nitrogen content, and 83 $mg(O_2).gTS^{-1}$ for COD. The histograms of obtained prediction values are presented in Figure 1.

2.2. Spectroscopic systems

The four spectroscopic systems compared in this study are presented below. In addition, spectral measurement protocols are compared in Table 1.

2.2.1. Laboratory spectroscopic system

The laboratory spectroscopic system consists of a NIR-Flex N-500 solids FT-NIR spectrophotometer with a vial accessory (Buchi, Flawil, Switzerland), scanning in reflectance mode with a spectral range of 4 000 cm^{-1} to 10 000 cm^{-1} (1000-2500 nm) and a resolution of 4 cm^{-1}. An external white reference (Spectralon®) signal $I_0(\lambda)$ is automatically taken every 10 minutes. For each sample, an intensity signal $I(\lambda)$ was collected, and the pseudo-absorbance signal $A_{lab}(\lambda)$ was computed:

$$A_{lab}(\lambda) = -log_{10}\left(R_{lab}(\lambda)\right) = -log_{10}\left(\frac{I(\lambda)}{I_0(\lambda)}\right). \quad \text{(Eq. 1)}$$

2.2.2. Portable spectrometer with immersed contact probe

The immersed contact probe system consists of a FT-NIR Rocket spectrometer (Arcoptix, Neuchatel, Switzerland) scanning in reflectance mode with a spectral range of 3 800 cm^{-1} to 11 000 cm^{-1} (900-2500 nm) and a resolution of 4 cm^{-1}. The spectrometer was connected to two optical fibers (for illumination and signal collection) of 1000 µm core diameter and numerical aperture of 0.39 (BFY1000, Thorlabs). A tungsten-halogen source (Ocean Optics HL-200-FHSA) was used for illumination. For each sample, the intensity $I(\lambda)$ was collected. A white reference (SRS99, Spectralon®) was scanned every hour during the measurements resulting in $I_0(\lambda)$. Finally, a dark current signal $I_n(\lambda)$ corresponding to the instrumental noise was recorded and subtracted to all spectra. A pseudo-absorbance signal $A_{ip}(\lambda)$ was thus calculated:

$$A_{ip}(\lambda) = -log_{10}\left(R_{ip}(\lambda)\right) = -log_{10}\left(\frac{I(\lambda) - I_n(\lambda)}{I_0(\lambda) - I_n(\lambda)}\right). \qquad \text{(Eq. 2)}$$

2.2.3. Portable spectrometer with polarized light spectroscopy

The polarized light system consists of the same elements (spectrometer, light source, optical fibers) as the immersed contact probe system, however, measurements were made at a distance of 5 cm from the samples, and a polarized light component (Awhangbo et al., 2020) was connected to the spectrometer. This component consisted in a wire-grid polarizer (Thorlabs WP25L-UB) to s-polarize the incident light; and a calcite Wolaston polarizer (Thorlabs WP10P) to split the reflected light in an s-polarized and p-polarized image, corresponding to parallel $I_{\parallel}(\lambda)$ and perpendicular $I_{\perp}(\lambda)$ light signals. As in the previous system, both the dark current signal $I_n(\lambda)$, and a white reference signal $I_0(\lambda) = I_{\parallel}(\lambda)_0 + I_{\perp}(\lambda)_0$ were collected. Three signals were then calculated following Bendoula et al. (2015) formula (Bendoula et al., 2015): the single scattering reflectance $R_{ss}(\lambda)$, the multiple scattering reflectance $R_{ms}(\lambda)$, and the total backscattering reflectance $R_{bs}(\lambda)$:

$$R_{ss}(\lambda) = \frac{(I_{\parallel}(\lambda) - I_n(\lambda)) - (I_{\perp}(\lambda) - I_n(\lambda))}{I_0(\lambda) - I_n(\lambda)}. \qquad \text{(Eq. 3)}$$

$$R_{ms}(\lambda) = \frac{2(I_{\perp}(\lambda) - I_n(\lambda))}{I_0(\lambda) - I_n(\lambda)}. \qquad \text{(Eq. 4)}$$

$$R_{bs}(\lambda) = \frac{(I_{\parallel}(\lambda) - I_n(\lambda)) + (I_{\perp}(\lambda) - I_n(\lambda))}{I_0(\lambda) - I_n(\lambda)}. \qquad \text{(Eq. 5)}$$

2.2.4. Handheld micro spectrometer

The micro spectrometer system consists of a MEMS FT-NIR NeoSpectra spectrometer (Si-Ware, Cairo, Egypt) scanning in reflectance mode with a spectral range of 3 921 cm^{-1} to 7 407 cm^{-1} (1350-2550 nm) and a resolution of 66 cm^{-1}. A white reference (SRS99, Spectralon®) signal $I_0(\lambda)$ was collected before each measurement. For each sample, an intensity signal $I(\lambda)$ was collected and the pseudo-absorbance signal $A_\mu(\lambda)$ was computed:

$$A_\mu(\lambda) = -log_{10}\left(R_\mu(\lambda)\right) = -log_{10}\left(\frac{I(\lambda)}{I_0(\lambda)}\right). \qquad \text{(Eq. 6)}$$

2.3. Data analysis: model calibration

All the data analysis was performed using Python 3.6.5: data wrangling with Pandas 0.25.1, NumPy 1.17.3, SciPy 1.3.1, Scikit-learn 0.21.3, and plotting with Matplotlib 2.2.2 (Harris et al., 2020; Hunter, 2007; McKinney, 2010; Pedregosa et al., 2015; van Rossum and Drake, 2009; Virtanen et al., 2020).

Measurements of the 33 substrates on the four spectroscopic configurations yielded six different matrices : the absorbance signal A_{lab} from the laboratory spectrometer, the absorbance signal A_{ip} from the immerged contact probe system, the three reflectance signals R_{ss}, R_{ms} and R_{bs} (respectively single scattered, multiple scattered, total back-scattered) from the polarized system, and finally the absorbance signal A_μ from the micro spectrometer system.

For noise reduction and baseline correction, a selection of seven pretreatments that have proven to be efficient in previous studies on organic waste (Charnier et al., 2017; Lesteur et al., 2011) have been used: the standard normal variate (Barnes et al., 1989) (SNV), the first-order detrend (Barnes et al., 1989) (DT1), the first-order Savitzky-Golay (Savitzky and Golay, 1964) derivation (SG1), the second-order Savitzky-Golay derivation (SG2), combinations of SNV and first-order Savitzky-Golay derivation (SNV+SG1 or SG1+SNV) and finally, a weighted EMSC with variable sorting for normalization (VSN) (Rabatel et al., 2020). The raw signal was used directly as well, which resulted overall in testing eight different preprocessing conditions.

In order to evaluate the models built on each spectroscopic system, a validation test set was constituted. With the aim of producing a representative validation test set, the Duplex algorithm (Snee, 1977) was run for each reference characteristic (carbohydrates content, lipid content, total nitrogen content, COD, BMP). This resulted in a training set of 22 substrates, and a validation test set of 11 substrates. To assess the representativeness of the validation test set in terms of spectral variability, a principal components analysis (Cordella, 2012) was done, and obtained scores were plot in Figure 2 and Appendix C.

Models were built using a partial least squares regression (PLS1-R) with NIPALS algorithm (Næs and Martens, 1984; WOLD, 1973). To determine the number of latent variables, a cross-validation was done using a repeated randomized group-k-fold cross-validation with $k = 5$ the fold number and $n\_repeats = 30$ the repetition number. Sample triplicates were always kept within one fold to ensure independence. For each cross-validation run, various metrics were then calculated: the root-mean-square error (RMSE), the mean absolute error (MAE) (Willmott and Matsuura, 2005), the coefficient of determination (R^2), and B-coefficients metrics which are the Durbin-Watson statistic (DW) and the variance (Rutledge and Barros, 2002). The choice of the number of latent variables was made by analyzing all these metrics together (i.e. choosing the minimal number of latent variables while minimizing RMSE and MAE, maximizing R^2, and detecting rate increase of DW and variance of B-coefficients).

Spectral range was also optimized for each of the signal types. This was done by calibrating a first model, analyzing its B-coefficients (available in Appendix E), and shrinking the spectral range adequately before recalibrating the model.

The final performances of the obtained models were evaluated on the validation test set, based on the root-mean-square error (RMSE) and the coefficient of determination (R^2).

To assess prediction repeatability of a given model, the variance of each sample's triplicate spectra predictions was calculated:

$$s_r^2 = \sum_{i=1}^{3} (\hat{y}_i - \bar{\hat{y}})^2, \qquad \text{(Eq. 7)}$$

and the global prediction repeatability standard deviation was calculated as the quadratic mean of each s_r:

$$S_r = \sqrt{\sum_{i=1}^{n\_test\_samples} s_{r\,i}^2}. \qquad \text{(Eq. 8)}$$

3. Results & Discussion

3.1. Data overview

3.1.1. Training set and validation test set

For each reference characteristic, train and test set distributions (respectively in blue and orange) are presented as histograms in Figure 1. Very similar distributions (same mean, same standard deviation) for all characteristics show that the Duplex algorithm succeeded in obtaining a representative test set in terms of biochemical composition. To complete this analysis, the representativeness in terms of signal is assessed by looking at the scores of train and test sets for each signal type in Figure 2 (only the first and second component scores are displayed, but scores up to the tenth component were checked). As shown, the test set signals (in orange) cover most of the range covered by train set signals. However, in some cases, the variability of train set signals is not fully well represented in the test set. For example, in the upper left score plot representing the laboratory spectrometer configuration signal A_{lab}, no test set signal (orange square) is found in the far right plot where there are two train set signals (blue triangles). This is consistent with the fact that the Duplex algorithm was run on the reference values and not on the spectral values, so there is no guarantee for test set spectral representativeness. Although this is not optimal for evaluating calibration models alone, such methodology appeared to be the best to compare different spectroscopic systems on identical samples without bias.

3.1.2. Raw spectra analysis

Figure 3 presents the raw reflectance signals obtained with each spectroscopic system. In all signals, the main peaks found in organic waste were apparent: the CH, CH_2 and CH_3 combination bands particularly present in fat (1731 nm, 1764 nm, 2310 nm, 2350 nm), the OH bands present in simple sugars (1436 nm, 1932 nm), the OH combination bands in starch or cellulose (2092 nm), and the NH combination bands present in proteins (2180 nm) (Williams and Antoniszyn, 2019; Workman Jr. and Weyer, 2012). However, the relative amplitude of these peaks seems to differ. For example, in the micro spectrometer signal (R_{μ}) the CH_2 combination bands at 2310 nm and 2350 nm seem much less sharp than in the laboratory spectrometer signal (R_{lab}). This can be well explained by the lower resolution of the micro-spectrometer (66 cm^{-1}) compared to the laboratory spectrometer (4 cm^{-1}). A consequence of this is that the models built on compact systems such as the micro spectrometer will be based on more simple features, which could lead them to be less accurate models but potentially also more robust.

In addition, the sensitivity with respect to the spectral range appears to differ from one spectrometer to another. For the micro spectrometer, the measured signal below 1600 nm seems much noisier than in other systems. Such sharp peaks are not, *a priori*, expected in NIR spectra of complex matter. Similarly, for the immersed probe contact (R_{ip}) or polarized signals (R_{ss}, R_{ms}, R_{bs}), it seems the measured signals below 1200 nm and over 2240 nm are as well very noisy. For this reason, these spectral regions were later removed from the calibration of the built models.

Another point of comparison concerns the observed reflectance levels (Figure 4). The reflectance levels of R_{lab}, R_{bs}, and R_{μ} are much higher (with 75% of the values that range respectively between 0.46 and 0.73, 0.43 and 0.66, and 0.60 and 0.90), than the reflectance levels of R_{ip} (with 75% of the values that range between 0.15 and 0.35). This is mostly related to the way the signal is acquired (i.e. the measurement configuration). Indeed, reflectance levels are the result of both the absorption level (dependent of chemical composition) and the scattering level (modifications of light optical path-length, and photon leakage (Gobrecht et al., 2014)). Therefore, the chosen measurement configuration might favour one or the other, leading to differences in the measured reflectance levels. Results show here that the distant mode systems (i.e. R_{lab}, R_{bs}, and R_{μ}) collect much more scattering photons than the contact mode system (i.e. R_{ip}). Regarding the advantage of one measurement mode over the other, this will mostly be dependent on the characteristic to be predicted, and its dependency on physical properties.

In the polarized light system, a clear difference of reflectance level can also be observed: 75% of the values of the multiple scattering signal R_{ms} range between 0.52 and 0.76, against 0.05 and 0.11 for the single scattering signal R_{ss}. This is consistent with the sole principle of polarized spectroscopy where R_{ss} corresponds to single scattering photons with low penetration in the media while R_{ms} corresponds to multiple scattering photons with a longer optical path length in the media due to refraction events. This further confirms the efficiency of polarized spectroscopy as an optical method to remove the scattering effects in the measured signal (Bendoula et al., 2015; Gobrecht et al., 2016). However, the impacts on the subsequent models built on such signals remain to be studied.

3.2. Model performances

For the five reference characteristics that were studied, the best selected models obtained on each of the six signals are presented in Table 2.

For prediction models built using the laboratory spectrometer system, the errors obtained on the test set (RMSEP) were of 0.108 $g.gTS^{-1}$ for carbohydrates content, 5.8 $mg.gTS^{-1}$ for nitrogen content, 0.034 $g.gTS^{-1}$ for lipids content, 0.060 $NL(CH_4).gTS^{-1}$ for BMP, and 136.4 $mg(O_2).gTS^{-1}$ for COD. These are all consistent to the performances of reference models (Charnier et al., 2017). The slightly lower performances obtained can be explained by the more limited number of samples on which these models were built (22 samples) compared to the original models (about 80 samples).

For all predicted characteristics, the laboratory system (A_{lab}) showed better analytical performance results than the compact systems (A_{ip}, A_{μ}, R_{ss}, R_{ms}, R_{bs}). However, in many cases, these latter systems showed similar performances to the laboratory system. For example, for BMP prediction, the prediction error (RMSEP) of the model obtained with the laboratory spectrometer signal A_{lab} was 60 mL(CH_4).gTS^{-1}. In comparison, for the polarized system signals R_{ss}, R_{ms}, R_{bs}, the model prediction errors were of respectively 115 mL(CH_4).gTS^{-1}, 111 mL(CH_4).gTS^{-1} and 100 mL(CH_4).gTS^{-1} , while for the micro spectrometer signal A_{μ} the model's error was of only 91 mL(CH_4).gTS^{-1}. Similarly, for carbohydrates content prediction, while the prediction error for the laboratory spectrometer was 0.108 g.gTS^{-1}, the errors for the micro-spectrometer and the immersed probe system were of only 0.134 g.gTS^{-1} and 0.104 g.gTS^{-1}. Such observation can be made for all the other characteristics studied. This is very promising because these models have acceptable errors compared to the laboratory spectrometer. This means that the models built on organic waste rely on sufficiently simple features so that the lower spectral resolution of compact spectrometers does not affect too much the performances. Such result is consistent with similar studies on low-cost compact NIR spectrometers with limited spectral range that are applied to herbaceous feedstock such as corn stover or sorghum (Wolfrum et al., 2020). Knowing that these spectrometers are low-cost (while the laboratory spectrometer costs about 50 000€, the immersed contact probe and polarized systems each cost about 20 000€ and the micro spectrometer only costs about 3 000 €), and can be used at-site, this holds great promises regarding an increased adoption of NIRS for robust solid organic waste characterization in anaerobic digestion plants.

Models built on the three signals R_{ss}, R_{ms}, R_{bs} obtained using the polarized spectroscopy system show different performances. While R_{bs} is a signal very similar to those obtained from the other set-ups because it includes information from all the backscattering light, R_{ss} and R_{ms} differ in terms of type of photons that are captured by the spectrometer (respectively single scattering photons, and multiple scattering photons). For all characteristics, models built on R_{bs} signal show better performances than models built on the R_{ss} and R_{ms} signals. For example, for COD prediction, while the prediction error (RMSEP) of the model using the total backscattering signal (R_{bs}) is of 129.2 mg(O_2).gTS^{-1}, it is of 147.8 mg(O_2).gTS^{-1} using R_{ms} and 273.9 mg(O_2).gTS^{-1} using R_{ss}. This suggests that the use of polarized spectroscopy for predicting these characteristics on organic waste may not be particularly recommended.

In fact, for lipids content, COD and nitrogen content, the models built with R_{ss} signals show much greater errors than models built with R_{ms} signals (respectively 0.124 g.gTS^{-1} greater than 0.068 g.gTS^{-1}, 273.9 mg(O_2).gTS^{-1} greater than 147.8 mg(O_2).gTS^{-1}, and 21.4 mg.gTS^{-1} greater than 12.1 mg.gTS^{-1}). This came as a surprise, as the single scattering signal is theoretically supposed to be more related to absorbing constituents and less impacted by scattering effects (Gobrecht et al., 2015). This can be explained by the fact that for a dataset with such diverse solid organic substrates, the biochemical composition is closely related to the physical properties. For example, high lipid content substrates (which also correspond to substrates with high COD) tend to form liquid transparent solutions (like oil), which transmit light much more than low lipid content substrates which usually form highly scattering porous media. This relatively poor performance obtained with the single scattering signal is consistent with results obtained on digestates where physical structure appeared determinant (Awhangbo et al., 2020). One additional reason can be found in the measurement technique itself: the intensity captured for the single scattering signal is much more limited than a classical total backscattering signal, leading to higher signal-to-noise ratios. Further investigations could concentrate on the use of a multi-block approach combining these three complementary signals, as proposed on digestates (Awhangbo et al., 2020).

Apart from the single scattering signal, all signals allowed to build satisfactory models for the biochemical characterization of organic waste. However, no spectroscopic system allowed to surpass the analytical performance of the laboratory spectrometer system. Figure 5 presents the observed and prediction plots for each signal for the prediction of biochemical potential. In A_{lab} (upper left subplot), the predictions for each of the three replicate spectra do not differ (for one observed value, the prediction values are overlaid on the graph); while for the other spectroscopic systems, the predictions for each of the three replicate spectra are very different. For example, the sample with a BMP of 0.63 $NL(CH_4)g.TS^{-1}$ has predictions that vary for A_{lab} between 0.869 $NL(CH_4)g.TS^{-1}$ and 0.870 $NL(CH_4)g.TS^{-1}$, while the predictions for A_{ip} and A_{μ} vary respectively between 0.863 $NL(CH_4)g.TS^{-1}$ and 0.940 $NL(CH_4)g.TS^{-1}$ and between 0.709 $NL(CH_4)g.TS^{-1}$ and 0.771 $NL(CH_4)g.TS^{-1}$. This is observed for all the other characteristics as shown in Appendix D. It appears that in all the compact systems, the replicate spectra vary much more from each other than with the laboratory spectrometer. This could explain the greater errors obtained using the compact systems. The following result may be investigated more quantitatively by calculating the global repeatability standard deviations as presented in Figure 6. Indeed, for all characteristics, the compact systems show much higher repeatability standard deviations than the laboratory spectrometer (in red). Such differences are due to the way the spectral measurements are acquired. As detailed in Table 1, the systems do not have the same number of scans and sampling surface. While for one measurement, the laboratory spectrometer collects scans during a full rotation of the sampling cup, the other systems only collect scans on a fixed point of the sample's surface. This means that in compact systems the spectral measurement is much less representative of the total sample. It appears that the performance of compact systems could be enhanced by optimizing the way the spectra are taken: increasing the number of scans and the number of replicates to ensure a better stability of the measurements.

While the suitability of the compact and low-cost spectrometers has been demonstrated, some challenges remain. Though models could be calibrated on the compact systems' signals directly as in this study, it is most probable that models will remain being built and maintained on standard laboratory spectrometers, with transfer functions being built between the laboratory spectrometer (referred as the "master" spectrometer) and the compact spectrometers (referred as the "slave" spectrometers). This transfer approach has already been proven to be successful between a laboratory spectrometer and an online spectrometer for in situ monitoring of anaerobic digestion (Krapf et al., 2013). However, the robustness of these transfer functions applied to compact systems still needs to be assessed.

4. Conclusions

Results have shown that compact and low-cost systems including a hand-held micro spectrometer are suitable for online characterization of diverse solid organic waste. However, the use of new measurement configurations such as the polarized mode was not shown to be an effective way to enhance the quality of predictive models. This suggests that the physical scattering properties of the substrates are the main determinant of analytical performance of NIRS calibration models built on such highly diverse solid organic waste. Keys for the improvement of the compact systems appear to lie in further optimization of the sampling protocol. These results set the path to a new era of low-cost and on-site NIRS analysis of the feeding substrates in co-digestion plants.

Acknowledgements

Financial support from the National Research Institute for Agriculture, Food and Environment (INRAE), the French Agency of National Research and Technology (ANRT) [grant number 2018/0461] and the Biogaz-RIO platform [FEDER-FSE Languedoc Roussillon 2014-2020] is hereby acknowledged.

References

Alayed, M., Deen, M.J., 2017. Time-resolved diffuse optical spectroscopy and imaging using solid-state detectors: Characteristics, present status, and research challenges. Sensors (Switzerland) 17, 2115. https://doi.org/10.3390/s17092115

Albrecht, R., Joffre, R., Gros, R., Le Petit, J., Terrom, G., Périssol, C., 2008. Efficiency of near-infrared reflectance spectroscopy to assess and predict the stage of transformation of organic matter in the composting process. Bioresour. Technol. 99, 448–455. https://doi.org/10.1016/j.biortech.2006.12.019

Awhangbo, L., Bendoula, R., Roger, J.M., Béline, F., 2020. Multi-block SO-PLS approach based on infrared spectroscopy for anaerobic digestion process monitoring. Chemom. Intell. Lab. Syst. 196, 103905. https://doi.org/10.1016/j.chemolab.2019.103905

Backman, V., Gurjar, R., Badizadegan, K., Itzkan, I., Dasari, R.R., Perelman, L.T., Feld, M.S., 1999. Polarized light scattering spectroscopy for quantitative measurement of epithelial cellular structures in situ. IEEE J. Sel. Top. Quantum Electron. 5, 1019–1026. https://doi.org/10.1109/2944.796325

Barnes, R.J., Dhanoa, M.S., Lister, S.J., 1989. Standard normal variate transformation and de-trending of near-infrared diffuse reflectance spectra. Appl. Spectrosc. 43, 772–777. https://doi.org/10.1366/0003702894202201

Beć, K.B., Grabska, J., Huck, C.W., 2021. Principles and Applications of Miniaturized Near-Infrared (NIR) Spectrometers. Chem. - A Eur. J. 27, 1514–1532. https://doi.org/10.1002/chem.202002838

Beć, K.B., Grabska, J., Siesler, H.W., Huck, C.W., 2020. Handheld near-infrared spectrometers: Where are we heading? NIR news 31, 28–35. https://doi.org/10.1177/0960336020916815

Bendoula, R., Gobrecht, A., Moulin, B., Roger, J.M., Bellon-Maurel, V., 2015. Improvement of the chemical content prediction of a model powder system by reducing multiple scattering using polarized light spectroscopy. Appl. Spectrosc. 69, 95–102. https://doi.org/10.1366/14-07539

Charnier, C., Latrille, E., Jimenez, J., Lemoine, M., Boulet, J.C., Miroux, J., Steyer, J.P., 2017. Fast characterization of solid organic waste content with near infrared spectroscopy in anaerobic digestion. Waste Manag. 59, 140–148. https://doi.org/10.1016/j.wasman.2016.10.029

Cordella, C.B.Y., 2012. PCA: The Basic Building Block of Chemometrics, in: Krull, I.S. (Ed.), Analytical Chemistry. IntechOpen, pp. 1–46. https://doi.org/10.5772/51429

Crocombe, R.A., 2018. Portable Spectroscopy. Appl. Spectrosc. 72, 1701–1751. https://doi.org/10.1177/0003702818809719

Dahm, K.D., Dahm, D.J., 2004. Relation of representative layer theory to other theories of diffuse reflection. J. Near Infrared Spectrosc. 12, 189–198. https://doi.org/10.1255/jnirs.426

Doublet, J., Boulanger, A., Ponthieux, A., Laroche, C., Poitrenaud, M., Cacho Rivero, J.A., 2013. Predicting the biochemical methane potential of wide range of organic substrates by near infrared spectroscopy. Bioresour. Technol. 128, 252–258. https://doi.org/10.1016/j.biortech.2012.10.044

Fitamo, T., Triolo, J.M., Boldrin, A., Scheutz, C., 2017. Rapid biochemical methane potential prediction of urban organic waste with near-infrared reflectance spectroscopy. Water Res. 119, 242–251. https://doi.org/10.1016/j.watres.2017.04.051

Gobrecht, A., Bendoula, R., Roger, J.M., Bellon-Maurel, V., 2016. A new optical method coupling light polarization and Vis-NIR spectroscopy to improve the measurement of soil carbon content. Soil Tillage Res. 155, 461–470.

https://doi.org/10.1016/j.still.2015.06.003

Gobrecht, A., Bendoula, R., Roger, J.M., Bellon-Maurel, V., 2015. Combining linear polarization spectroscopy and the Representative Layer Theory to measure the Beer-Lambert law absorbance of highly scattering materials. Anal. Chim. Acta 853, 486–494. https://doi.org/10.1016/j.aca.2014.10.014

Gobrecht, A., Roger, J.M., Bellon-Maurel, V., 2014. Major Issues of Diffuse Reflectance NIR Spectroscopy in the Specific Context of Soil Carbon Content Estimation. A Review., Advances in Agronomy. https://doi.org/10.1016/B978-0-12-420225-2.00004-2

Godin, B., Mayer, F., Agneessens, R., Gerin, P., Dardenne, P., Delfosse, P., Delcarte, J., 2015. Biochemical methane potential prediction of plant biomasses: Comparing chemical composition versus near infrared methods and linear versus non-linear models. Bioresour. Technol. 175, 382–390. https://doi.org/10.1016/j.biortech.2014.10.115

Hagos, K., Zong, J., Li, D., Liu, C., Lu, X., 2017. Anaerobic co-digestion process for biogas production: Progress, challenges and perspectives. Renew. Sustain. Energy Rev. 76, 1485–1496. https://doi.org/10.1016/j.rser.2016.11.184

Harris, C.R., Millman, K.J., van der Walt, S.J., Gommers, R., Virtanen, P., Cournapeau, D., Wieser, E., Taylor, J., Berg, S., Smith, N.J., Kern, R., Picus, M., Hoyer, S., van Kerkwijk, M.H., Brett, M., Haldane, A., del Río, J.F., Wiebe, M., Peterson, P., Gérard-Marchant, P., Sheppard, K., Reddy, T., Weckesser, W., Abbasi, H., Gohlke, C., Oliphant, T.E., 2020. Array programming with NumPy. Nature 585, 357–362. https://doi.org/10.1038/s41586-020-2649-2

Hemrattrakun, P., Nakano, K., Boonyakiat, D., Ohashi, S., Maniwara, P., Theanjumpol, P., Seehanam, P., 2021. Comparison of Reflectance and Interactance Modes of Visible and Near-Infrared Spectroscopy for Predicting Persimmon Fruit Quality. Food Anal. Methods 14, 117–126. https://doi.org/10.1007/s12161-020-01853-w

Hunter, J.D., 2007. Matplotlib: A 2D graphics environment. Comput. Sci. Eng. 9, 90–95. https://doi.org/10.1109/MCSE.2007.55

Jacobi, H.F., Moschner, C.R., Hartung, E., 2011. Use of near infrared spectroscopy in online-monitoring of feeding substrate quality in anaerobic digestion. Bioresour. Technol. 102, 4688–4696. https://doi.org/10.1016/j.biortech.2011.01.035

Jacobi, H.F., Moschner, C.R., Hartung, E., 2009. Use of near infrared spectroscopy in monitoring of volatile fatty acids in anaerobic digestion. Water Sci. Technol. 60, 339–346. https://doi.org/10.2166/wst.2009.345

Jacobi, H.F., Ohl, S., Thiessen, E., Hartung, E., 2012. NIRS-aided monitoring and prediction of biogas yields from maize silage at a full-scale biogas plant applying lumped kinetics. Bioresour. Technol. 103, 162–172. https://doi.org/10.1016/j.biortech.2011.10.012

Johansson, J., Folestad, S., Josefson, M., Sparen, A., Abrahamsson, C., Andersson-Engels, S., Svanberg, S., 2002. Time-resolved NIR/vis spectroscopy for analysis of solids: Pharmaceutical tablets. Appl. Spectrosc. 56, 725–731. https://doi.org/10.1366/000370202760077676

Khodabakhshian, R., Emadi, B., Khojastehpour, M., Golzarian, M.R., 2019. A comparative study of reflectance and transmittance modes of Vis/NIR spectroscopy used in determining internal quality attributes in pomegranate fruits. J. Food Meas. Charact. 13, 3130–3139. https://doi.org/10.1007/s11694-019-00235-z

Krapf, L.C., Nast, D., Gronauer, A., Schmidhalter, U., Heuwinkel, H., 2013. Transfer of a near infrared spectroscopy laboratory application to an online process analyser for in situ monitoring of anaerobic digestion. Bioresour. Technol. 129, 39–50.

https://doi.org/10.1016/j.biortech.2012.11.027

Lesteur, M., Latrille, E., Maurel, V.B., Roger, J.M., Gonzalez, C., Junqua, G., Steyer, J.P., 2011. First step towards a fast analytical method for the determination of Biochemical Methane Potential of solid wastes by near infrared spectroscopy. Bioresour. Technol. 102, 2280–2288. https://doi.org/10.1016/j.biortech.2010.10.044

Lomborg, C.J., Holm-Nielsen, J.B., Oleskowicz-Popiel, P., Esbensen, K.H., 2009. Near infrared and acoustic chemometrics monitoring of volatile fatty acids and dry matter during co-digestion of manure and maize silage. Bioresour. Technol. 100, 1711–1719. https://doi.org/10.1016/j.biortech.2008.09.043

Mallet, A., Charnier, C., Latrille, É., Bendoula, R., Steyer, J.-P., Roger, J.-M., 2021. Unveiling non-linear water effects in near infrared spectroscopy: A study on organic wastes during drying using chemometrics. Waste Manag. 122, 36–48. https://doi.org/10.1016/j.wasman.2020.12.019

McKinney, W., 2010. Data Structures for Statistical Computing in Python, in: Proceedings of the 9th Python in Science Conference. pp. 56–61. https://doi.org/10.25080/majora-92bf1922-00a

McVey, C., McGrath, T.F., Haughey, S.A., Elliott, C.T., 2021. A rapid food chain approach for authenticity screening: The development, validation and transferability of a chemometric model using two handheld near infrared spectroscopy (NIRS) devices. Talanta 222, 121533. https://doi.org/10.1016/j.talanta.2020.121533

Næs, T., Martens, H., 1984. Multivariate calibration. II. Chemometric methods. Trends Anal. Chem. 3, 266–271. https://doi.org/10.1016/0165-9936(84)80044-8

Pedregosa, F., Varoquaux, G., Buitinck, L., Louppe, G., Grisel, O., Mueller, A., 2015. Scikit-learn: Machine Learning in Python. J. Mach. Learn. Res. 19, 29–33.

Rabatel, G., Marini, F., Walczak, B., Roger, J.M., 2020. VSN: Variable sorting for normalization. J. Chemom. 34, 1–16. https://doi.org/10.1002/cem.3164

Rinnan, Å., Berg, F. van den, Engelsen, S.B., 2009. Review of the most common pre-processing techniques for near-infrared spectra. TrAC - Trends Anal. Chem. 28, 1201–1222. https://doi.org/10.1016/j.trac.2009.07.007

Rodrigues, R.P., Rodrigues, D.P., Klepacz-Smolka, A., Martins, R.C., Quina, M.J., 2019. Comparative analysis of methods and models for predicting biochemical methane potential of various organic substrates. Sci. Total Environ. 649, 1599–1608. https://doi.org/10.1016/j.scitotenv.2018.08.270

Rutledge, D.N., Barros, A.S., 2002. Durbin-Watson statistic as a morphological estimator of information content. Anal. Chim. Acta 454, 277–295. https://doi.org/10.1016/S0003-2670(01)01555-0

Savitzky, A., Golay, M.J.E., 1964. Smoothing and Differentiation of Data by Simplified Least Squares Procedures. Anal. Chem. 36, 1627–1639. https://doi.org/10.1021/ac60214a047

Schaare, P.N., Fraser, D.G., 2000. Comparison of reflectance, interactance and transmission modes of visible-near infrared spectroscopy for measuring internal properties of kiwifruit (Actinidia chinensis). Postharvest Biol. Technol. 20, 175–184. https://doi.org/10.1016/S0925-5214(00)00130-7

Sharififar, A., Singh, K., Jones, E., Ginting, F.I., Minasny, B., 2019. Evaluating a low-cost portable NIR spectrometer for the prediction of soil organic and total carbon using different calibration models. Soil Use Manag. 35, 607–616. https://doi.org/10.1111/sum.12537

Skvaril, J., Kyprianidis, K.G., Dahlquist, E., 2017. Applications of near-infrared spectroscopy (NIRS) in biomass energy conversion processes: A review. Appl. Spectrosc. Rev. 52, 675–728. https://doi.org/10.1080/05704928.2017.1289471

Snee, R.D., 1977. Validation of Regression Models: Methods and Examples. Technometrics 19, 415–428. https://doi.org/10.1080/00401706.1977.10489581

Stockl, A., Lichti, F., 2018. Near-infrared spectroscopy (NIRS) for a real time monitoring of the biogas process. Bioresour. Technol. 247, 1249–1252. https://doi.org/10.1016/j.biortech.2017.09.173

Tang, Y., Jones, E., Minasny, B., 2020. Evaluating low-cost portable near infrared sensors for rapid analysis of soils from South Eastern Australia. Geoderma Reg. 20, e00240. https://doi.org/10.1016/j.geodrs.2019.e00240

Triolo, J.M., Ward, A.J., Pedersen, L., Løkke, M.M., Qu, H., Sommer, S.G., 2014. Near Infrared Reflectance Spectroscopy (NIRS) for rapid determination of biochemical methane potential of plant biomass. Appl. Energy 116, 52–57. https://doi.org/10.1016/j.apenergy.2013.11.006

van Rossum, G., Drake, F.L., 2009. Python 3 Reference Manual, CreateSpace. Scotts Valley, CA. https://doi.org/10.5555/1593511

Vergnoux, A., Guiliano, M., Le Dréau, Y., Kister, J., Dupuy, N., Doumenq, P., 2009. Monitoring of the evolution of an industrial compost and prediction of some compost properties by NIR spectroscopy. Sci. Total Environ. 407, 2390–2403. https://doi.org/10.1016/j.scitotenv.2008.12.033

Virtanen, P., Gommers, R., Oliphant, T.E., Haberland, M., Reddy, T., Cournapeau, D., Burovski, E., Peterson, P., Weckesser, W., Bright, J., van der Walt, S.J., Brett, M., Wilson, J., Millman, K.J., Mayorov, N., Nelson, A.R.J., Jones, E., Kern, R., Larson, E., Carey, C.J., Polat, İ., Feng, Y., Moore, E.W., VanderPlas, J., Laxalde, D., Perktold, J., Cimrman, R., Henriksen, I., Quintero, E.A., Harris, C.R., Archibald, A.M., Ribeiro, A.H., Pedregosa, F., van Mulbregt, P., Vijaykumar, A., Bardelli, A. Pietro, Rothberg, A., Hilboll, A., Kloeckner, A., Scopatz, A., Lee, A., Rokem, A., Woods, C.N., Fulton, C., Masson, C., Häggström, C., Fitzgerald, C., Nicholson, D.A., Hagen, D.R., Pasechnik, D. V., Olivetti, E., Martin, E., Wieser, E., Silva, F., Lenders, F., Wilhelm, F., Young, G., Price, G.A., Ingold, G.L., Allen, G.E., Lee, G.R., Audren, H., Probst, I., Dietrich, J.P., Silterra, J., Webber, J.T., Slavič, J., Nothman, J., Buchner, J., Kulick, J., Schönberger, J.L., de Miranda Cardoso, J.V., Reimer, J., Harrington, J., Rodríguez, J.L.C., Nunez-Iglesias, J., Kuczynski, J., Tritz, K., Thoma, M., Newville, M., Kümmerer, M., Bolingbroke, M., Tartre, M., Pak, M., Smith, N.J., Nowaczyk, N., Shebanov, N., Pavlyk, O., Brodtkorb, P.A., Lee, P., McGibbon, R.T., Feldbauer, R., Lewis, S., Tygier, S., Sievert, S., Vigna, S., Peterson, S., More, S., Pudlik, T., Oshima, T., Pingel, T.J., Robitaille, T.P., Spura, T., Jones, T.R., Cera, T., Leslie, T., Zito, T., Krauss, T., Upadhyay, U., Halchenko, Y.O., Vázquez-Baeza, Y., 2020. SciPy 1.0: fundamental algorithms for scientific computing in Python. Nat. Methods 17, 261–272. https://doi.org/10.1038/s41592-019-0686-2

Williams, P., Antoniszyn, J., 2019. Near-infrared Technology: Getting the best out of light. African Sun Media. https://doi.org/10.18820/9781928480310

Willmott, C.J., Matsuura, K., 2005. Advantages of the mean absolute error (MAE) over the root mean square error (RMSE) in assessing average model performance. Clim. Res. 30, 79–82. https://doi.org/10.3354/cr030079

WOLD, H., 1973. Nonlinear Iterative Partial Least Squares (NIPALS) Modelling: Some Current Developments, Multivariate Analysis–III. Academic press, Inc. https://doi.org/10.1016/b978-0-12-426653-7.50032-6

Wolf, D., von Canstein, H., Schröder, C., 2011. Optimisation of biogas production by infrared spectroscopy-based process control. J. Nat. Gas Sci. Eng. 3, 625–632. https://doi.org/10.1016/j.jngse.2011.07.006

Wolfrum, E.J., Payne, C., Schwartz, A., Jacobs, J., Kressin, R.W., 2020. A Performance

Comparison of Low-Cost Near-Infrared (NIR) Spectrometers to a Conventional Laboratory Spectrometer for Rapid Biomass Compositional Analysis. Bioenergy Res. https://doi.org/10.1007/s12155-020-10135-6

Workman Jr., J., Weyer, L., 2012. Practical Guide and Spectral Atlas for Interpretive Near-Infrared Spectroscopy. CRC press. https://doi.org/10.1201/b11894

Wu, D., Li, L., Zhao, X., Peng, Y., Yang, P., Peng, X., 2019. Anaerobic digestion: A review on process monitoring. Renew. Sustain. Energy Rev. 103, 1–12. https://doi.org/10.1016/j.rser.2018.12.039

Xu, J.L., Gobrecht, A., Gorretta, N., Héran, D., Gowen, A.A., Bendoula, R., 2019. Development of a polarized hyperspectral imaging system for investigation of absorption and scattering properties. J. Near Infrared Spectrosc. 27, 314–329. https://doi.org/10.1177/0967033519857732

Yang, G., Li, Y., Zhen, F., Xu, Y., Liu, J., Li, N., Sun, Y., Luo, L., Wang, M., Zhang, L., 2021. Biochemical methane potential prediction for mixed feedstocks of straw and manure in anaerobic co-digestion. Bioresour. Technol. 326, 124745. https://doi.org/10.1016/j.biortech.2021.124745

Zeaiter, M., Roger, J.M., Bellon-Maurel, V., 2005. Robustness of models developed by multivariate calibration. Part II: The influence of pre-processing methods. TrAC - Trends Anal. Chem. 24, 437–445. https://doi.org/10.1016/j.trac.2004.11.023

Tables

Table 1. Spectral measurement protocol characteristics.

	Laboratory spectrometer	**Immersed contact probe**	**Polarization system**	**Micro spectrometer**
Measurement replicates	3	3	3	3
Number of scans per measurement	96 scans	10 scans	10 scans	28s scan time
Measurement sampling method (measured area per scan)	360° rotation (~5 cm^2)	Fixed point (~0.05 cm^2)	Fixed point (~1 cm^2)	Fixed point (~25 cm^2)
Protocol between replicates	Mix the whole sample	Change the measured surface position	Change the measured surface position	Change the measured surface position

Table 2. Descriptive statistics of the calibrated models. For each predicted reference measurement (carbohydrates, nitrogen, lipids, BMP, COD), the retained model for each spectroscopic system signal (A_{lab}, A_{ip}, A_{μ}, R_{ss}, R_{ms}, R_{bs}) is presented. The optimized parameters are provided (the spectral range, the pretreatment and the number of latent variables) along with the different performance metrics (RMSEC, RMSECV, RMSEP, R^2C, R^2P).

Experiment		**Optimized parameters**			**Performance metrics**				
Reference	**Signal**	**Spectral range (nm)**	**Pretreatment**	**#LV**	**$RMSE_C$**	**$RMSE_{CV}$**	**$RMSE_P$**	**R^2_C**	**R^2_P**
Carbohydrates	**A_{lab}**	1400-2240	SNV+SG1	2	0.143	0.192	0.108	0.78	0.83
$g.gTS^{-1}$	**A_{ip}**	1450-2240	SNV	2	0.188	0.169	0.104	0.82	0.84
	A_u	1400-2500	SNV+SG1	3	0.146	0.137	0.134	0.75	0.88
	R_{ss}	1200-2240	SNV	2	0.259	0.296	0.207	0.28	0.37
	R_{ms}	1200-2240	Raw	4	0.121	0.185	0.112	0.82	0.82
	R_{bs}	1300-2300	SNV+SG1	3	0.119	0.158	0.130	0.74	0.91
Nitrogen	**A_{lab}**	1200-2240	SNV+SG1	10	3.6	15.0	5.8	0.98	0.89
$mg.gTS^{-1}$	**A_{ip}**	1200-2240	SNV+SG1	5	9.9	18.4	7.5	0.87	0.83
	A_u	1400-2500	SNV	5	10.1	20.7	13.1	0.85	0.51
	R_{ss}	1200-2240	SG2	3	17.2	23.1	21.4	0.62	-0.4
	R_{ms}	1200-2240	SNV+SG1	5	12.6	22.6	12.1	0.80	0.54
	R_{bs}	1300-2300	SG1+SNV	4	10.7	17.6	11.7	0.83	0.61
Lipids	**A_{lab}**	1400-2240	SNV	6	0.025	0.056	0.034	0.99	0.98
$g.gTS^{-1}$	**A_{ip}**	1200-2240	VSN	9	0.057	0.066	0.066	0.99	0.93
	A_u	1400-2500	SG1+SNV	6	0.039	0.081	0.067	0.98	0.92
	R_{ss}	1200-2240	Raw	5	0.084	0.110	0.124	0.91	0.74
	R_{ms}	1200-2240	SG2	5	0.029	0.059	0.068	0.99	0.92

	R_{bs}	1200-2480	SG2	6	0.029	0.066	0.066	0.99	0.93
BMP	**A_{lab}**	1400-2240	SNV+SG1	9	0.020	0.078	0.060	0.99	0.90
$NL(CH_4).gTS^{-1}$	**A_{ip}**	1200-2240	SG1	2	0.088	0.115	0.110	0.77	0.73
	A_u	1600-2500	SG2	2	0.102	0.109	0.091	0.74	0.82
	R_{ss}	1200-2240	SG1	4	0.085	0.115	0.115	0.79	0.71
	R_{ms}	1350-2240	SG1	3	0.087	0.115	0.111	0.78	0.73
	R_{bs}	1300-2300	SG1	6	0.046	0.120	0.100	0.94	0.78
COD	**A_{lab}**	1400-2240	SNV	6	63.0	186.8	136.4	0.97	0.94
$mg(O_2).gTS^{-1}$	**A_{ip}**	1450-2240	SNV+SG1	7	106.2	228.3	160.2	0.93	0.90
	A_u	1400-2500	SG1+SNV	3	180.4	303.1	196.9	0.81	0.85
	R_{ss}	1200-2240	SG2	4	192.0	247.4	273.9	0.78	0.72
	R_{ms}	1350-2240	SG1	3	112.5	151.4	147.8	0.92	0.92
	R_{bs}	1200-2480	SG1+SNV	4	128.1	237.6	129.2	0.90	0.94

Figures

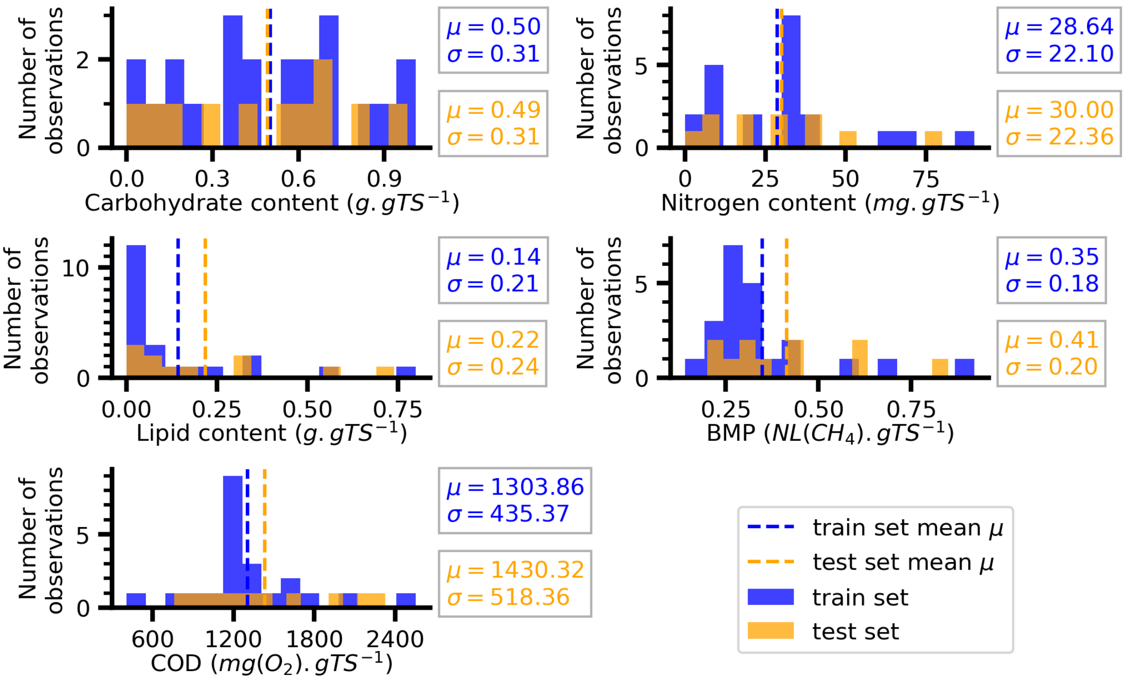

Figure 1. Histograms of reference characteristics. Both train and test sets (respectively in blue and in orange) obtained by a Duplex split are presented. Respective mean (labeled as μ) and standard deviation (labeled as σ) are presented for train and test sets (respectively in blue, and in orange). Dotted lines represent respective mean values.

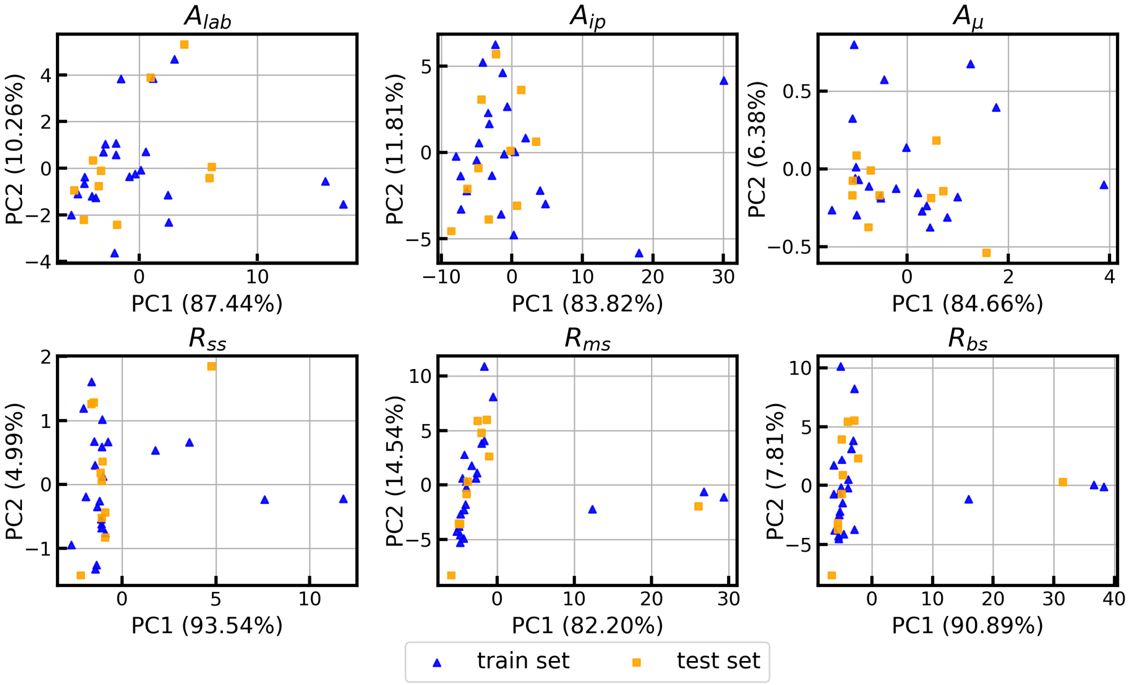

Figure 2. Principal component analysis (PCA) score plots of train and test sets (respectively in blue triangles, and in orange squares) for each signal type (from the four spectroscopic configurations). Each subplot represents the scores of the first and second principal components (PC1 and PC2). The percentage of explained variance is provided in the labels. The train and test split was obtained by a Duplex split based on the carbohydrates content levels. Score plots for other reference characteristics are shown in Appendix C.

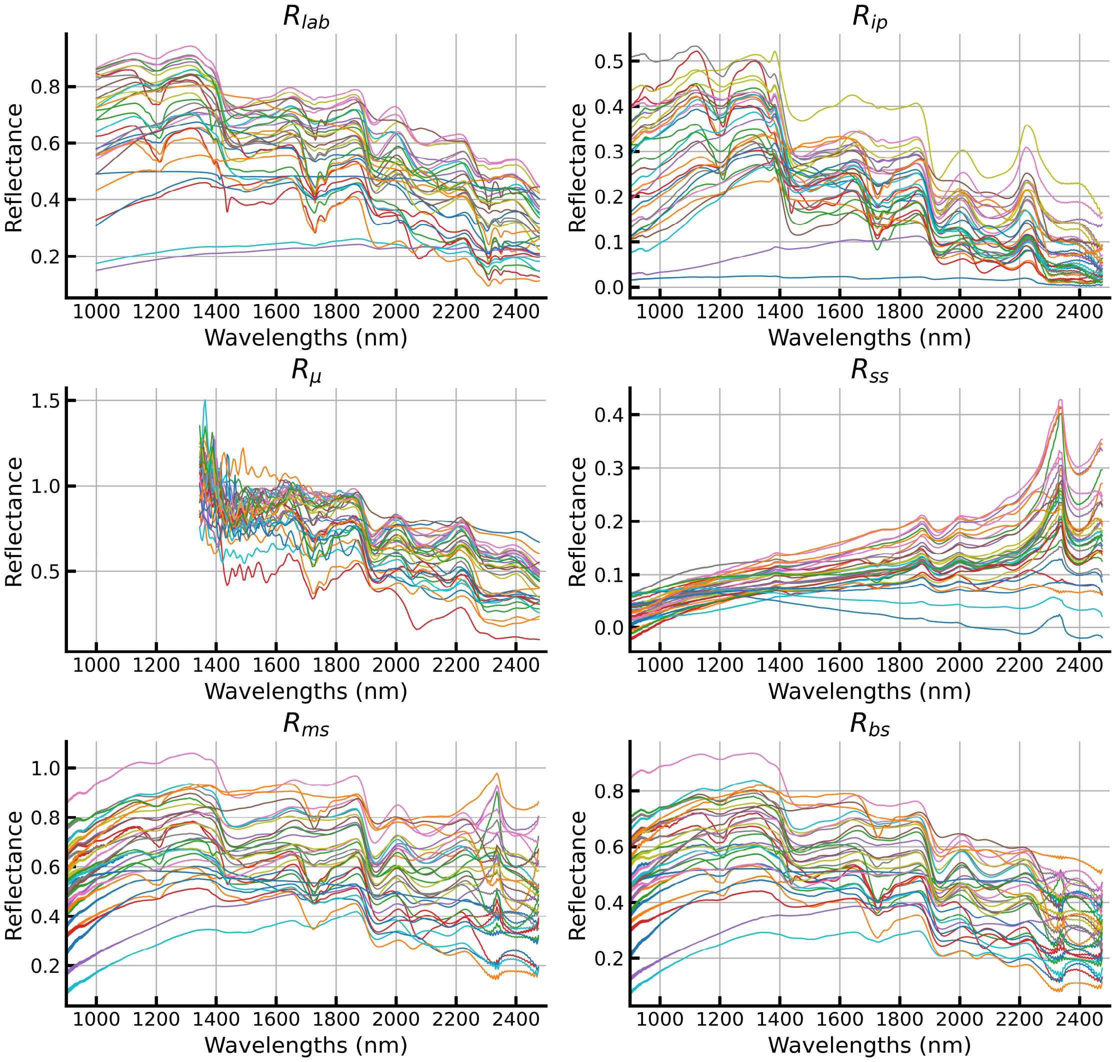

Figure 3. Raw reflectance spectra of each spectroscopic system (R_{lab}: laboratory spectrometer, R_{ip}: immersed probe system, R_{μ}: micro-spectrometer, R_{ss}: single scattered signal of polarized system, R_{ms}: multiple scattered signal of polarized system, R_{bs}: total backscattered signal of polarized system). Each spectrum corresponds to the mean of the triplicate measurements.

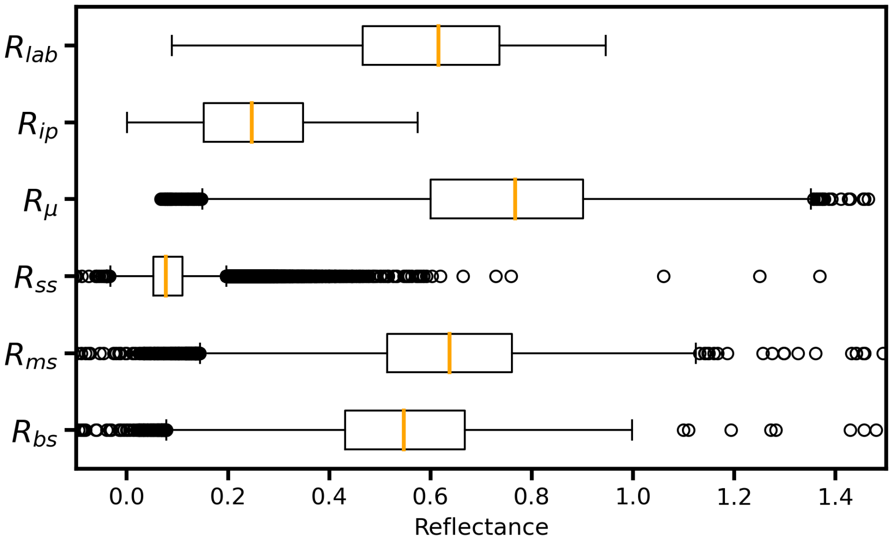

Figure 4. Boxplots of raw reflectance spectra values for each signal type (R_{lab}: laboratory spectrometer, R_{ip}: immersed probe system, R_{μ}: micro-spectrometer, R_{ss}: single scattered signal of polarized system, R_{ms}: multiple scattered signal of polarized system, R_{bs}: total back-scattered signal of polarized system). Each boxplot was obtained on the flattened matrix (reflectance values for all samples and for all wavelengths). Median values are presented with orange lines. The box limits represent the first and third quartile values (respectively $Q1$ and $Q3$), and the lines that extend from the box show the lowest and largest data points excluding any outliers (respectively $Q1 - 1.5 \times (Q3 - Q1)$ and $Q1 - 1.5 \times (Q3 - Q1)$). Outliers are presented in empty black circles.

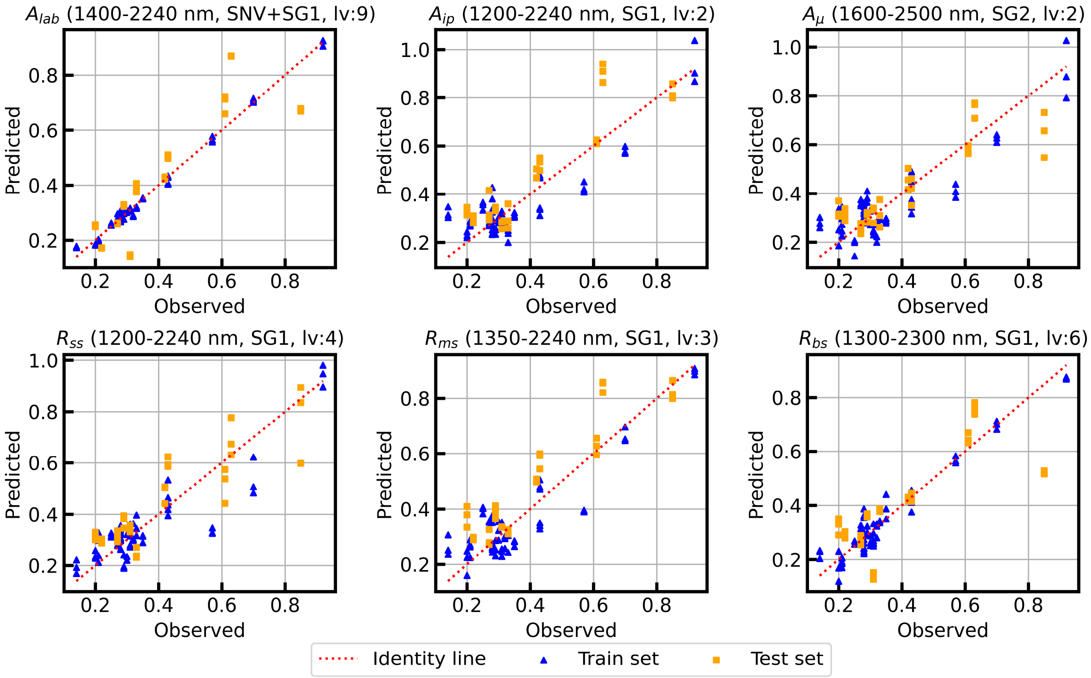

Figure 5. Scatter plots of predicted and observed values for the selected prediction models of biochemical methane potential (BMP). Each subplot corresponds to the best model selected for a signal type (from the four spectroscopic configurations). Values for train and test sets are respectively presented in blue triangles and orange squares. The spectral range, pre-processing type and latent variable number (lv) of the models are provided in the titles. Results for other reference characteristics are provided in Appendix D.

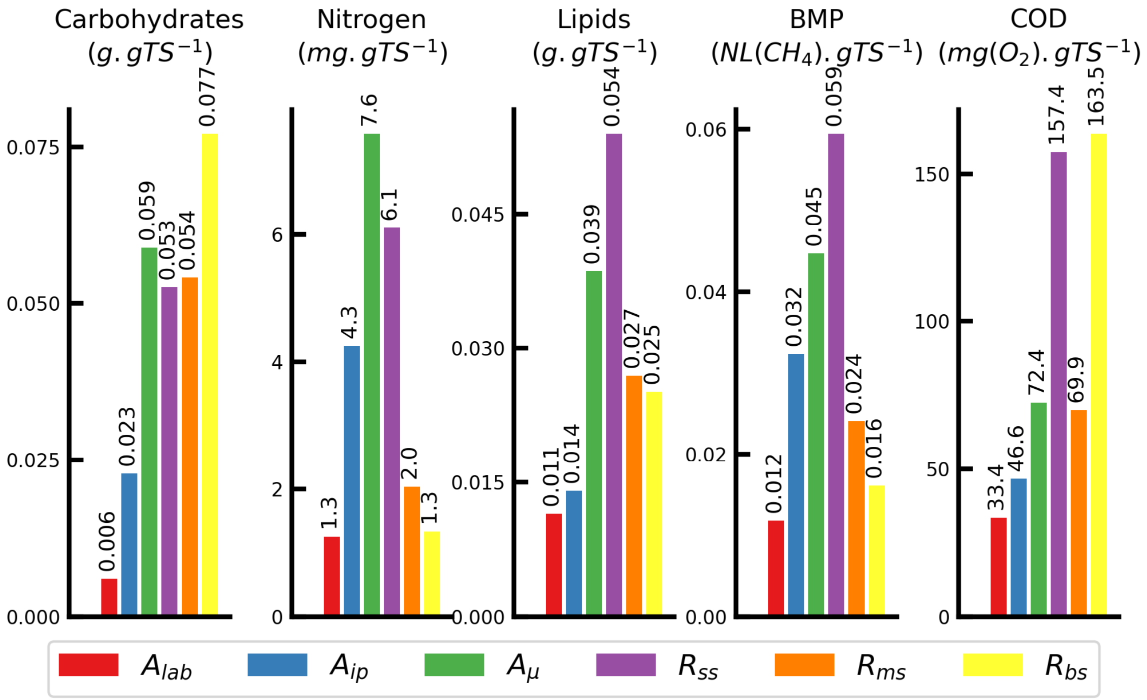

Figure 6. Global prediction repeatability standard deviations as calculated with (Eq. 7) and (Eq. 8). For each reference characteristic (carbohydrates, nitrogen, lipids, BMP, COD), a bar plot colored by signal type is provided (A_{lab} in red, A_{ip} in blue, A_{μ} in green, R_{ss} in violet, R_{ms} in orange, and R_{bs} in yellow).

Graphical abstract

1

Biochemical characterization of **diverse organic wastes**

2

Evaluation of **different spectroscopic systems for at-line use**

Different **compactness**

- Benchtop
- Portable
- Micro-spectrometer

Different **measurement types**

- Contact/Distance
- Polarized light

3

Comparison of **model performances**

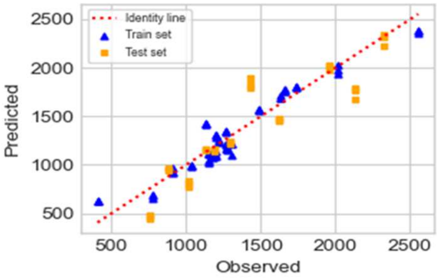

Graphical Abstract - Various organic wastes substrates were collected (1), and spectra were acquired on four different spectroscopic systems (2) with different compactness and measurement types. Then, calibration models were built on each of these spectroscopic systems (3) to predict five different biochemical characteristics (BMP, DCO, Sugar, Nitrogen, Lipids). The spectroscopic systems were compared and evaluated based on the performances of these models.